IOP Conf. Series: Journal of Physics: Conf. Series **1256** (2019) 012008 doi:10.1088/1742-6596/1256/1/012008

Evaluation of Wind Speed Retrieval from Continuous-Wave Lidar Measurements of a Wind Turbine Wake Using Virtual Lidar Techniques

M. Debnath[1], P. Doubrawa[1], T. Herges[2], L.A. Martínez-Tossas[1], D.C. Maniaci[2], P. Moriarty[1]

[1] National Renewable Energy Laboratory, National Wind Technology Center, Colorado, USA
[2] Sandia National Laboratories, Albuquerque, New Mexico, USA

E-mail: mithu.debnath@nrel.gov

Abstract. Wind lidar technology is being extensively used in utility-scale wind turbine wake measurements because of its capabilities to capture the dominant structures of interest in the near-wake region. However, wind lidar devices provide only line-of-sight (LOS) measurements, and retrieval of horizontal wind speed from the LOS measurements of a single lidar in the wind turbine wake could introduce errors due to the assumptions used in the retrieval process. With that in mind, the goals of this paper are to estimate the errors associated with the retrieval processes and provide guidelines for best practices. To achieve these goals, virtual lidar samples are obtained with large-eddy simulations (LES) by sampling the flow field with a model of the Technical University of Denmark (DTU) SpinnerLidar. LES is chosen to simulate the neutral and unstable atmospheric boundary layer (ABL), a benchmark case of the International Energy Agency Wind Technology Collaboration Programme (IEA Wind TCP) Task 31. The precursor ABL simulation is validated with the reference data provided by the IEA Wind Task 31 benchmark case. The data from the precursor simulation is used to drive a simulation of a wind turbine submerged in the ABL. A weighting function is applied to the LES data to mimic the real DTU SpinnerLidar measurements. In the end, the virtual lidar data are processed and compared with the original LES data to estimate the errors. Results show that lidar captures mean ABL profile without any noticeable error, whereas turbulence intensity is underpredicted $\approx 15\%$ at hub height for the neutral case. Volume averaging by the lidar technology has a significant effect in the shear layer of a wind turbine wake.

1. Introduction

Conventional meteorological towers ("met masts") are equipped with cup and sonic anemometers and therefore can only provide *in situ* measurements of wind speed. However, wind in the atmospheric boundary layer is dynamic and three dimensional, warranting measurements not only at a single point but along multiple dimensions. When it comes to wind turbine wakes, understanding complex turbulence patterns becomes critical, as they ultimately affect the performance and reliability of wind plants. The need for remote, multipoint observations has driven remote-sensing technology, particularly lidars, to increased levels of popularity in the wind industry in recent years. Lidars are able to perform multipoint measurements remotely without affecting the flow by their presence. This multipoint measurement technique can be used

to measure the evolution of the wind coming to a turbine or of its wake at different downstream locations.

Despite the clear advantages of lidar over conventional anemometry, lidars also have limitations of their own. Lidar technology is based on the Doppler effect and uses backscattered signals from aerosols in the atmosphere to estimate the wind speed parallel to the laser beam. Therefore, it is only able to estimate the wind speed along the "line of sight" (LOS) of the laser. This wind speed is proportional to the frequency of the Doppler shift in the returned signal. Calculating the peak frequency requires a considerable number of backscattered signals and, as a result, the LOS velocity is approximated over a larger volume as opposed to a fixed point, as provided by a sonic or cup anemometer. Because lidars cannot measure the three-dimensional wind vector, inflow and wake measurements performed with lidars cannot be directly used to validate wake models. Multiple lidars might provide a solution toward obtaining more velocity components from LOS data, but this application faces some challenges related to the speed of the lidar scanning head and its ability to change the measurement location, as well as synchronization among different lidars [1] and intersections of measurement volume from different instruments.

Retrieving horizontal wind speed from LOS measurements obtained with a single lidar requires some assumptions [2], which lead to additional measurement uncertainty. When using lidar measurements for model validation, it is important to understand how these and other sources of uncertainty (e.g., volume averaging [3, 4]) affect the estimated velocities. Work has been done to quantify these uncertainties relative to cup and sonic anemometers measurements when lidars are used to measure atmospheric boundary layer (ABL) profiles [5]. However, lidar measurements of wind turbine wakes have not been well-examined in that regard, mainly due to the unavailability of the traditional reference instruments and to the additional challenges that lidars face when measuring wakes, such as higher vertical velocity values. Projection of vertical velocity equal to zero might introduce a substantial error in the retrieval process.

Lidar measurements might have errors associated with the changes in wind direction and turbine operating conditions due to the lower rate of movement of the scanning head compared to the atmospheric turbulence. Errors resulting from the retrieval process and the lidar technology itself cannot be easily separated in real-world measurements, as wind direction and turbine operation data have their own uncertainties. The solution is to perform a computational fluid dynamics (CFD) experiment: an ideal flow field with known turbulence and wind direction is generated and sampled by a "virtual lidar" that sees both the actual velocity components and the LOS equivalent [6]. Through a detailed study with a virtual lidar, biases and errors of the physical measurement technique can be determined [7].

In this work, CFD is used [8] to further the understanding of specific limitations of scanning lidars when measuring wind turbine wakes [9]. We consider the DTU SpinnerLidar [10], which uses a continuous-wave laser and has the ability to sample the flow in three-dimensional space much faster than pulse-based lidars. However, even if they are able to measure fast, the measurement quality might deteriorate at longer focus distances due to the increase of sampling with focus distances.

Based on the discussed limitations of lidars, three main questions are asked in this work: 1) what is the accuracy of continuous-wave lidar measurements in the far wake of a wind turbine, where the probe volume is larger? 2) can we retrieve horizontal wind speed from LOS data, while assuming the projection of vertical velocity in the horizontal plane to be zero? and, 3) how does atmospheric stability affect the wind speed retrieval process? These questions are addressed by creating a virtual lidar in a CFD simulation that mimics the operation of the real-world SpinnerLidar. The atmospheric inflow is based on the wake model validation benchmarks of the IEA Wind Task 31 SWiFT benchmark [11] released by the National Renewable Energy Laboratory (NREL). Considering these perspectives, this paper is organized as follows: the CFD simulations for the benchmark cases are discussed in Section 2, and the virtual lidar incorporated

in the CFD model is discussed in Section 3. Results analysis is provided in Section 4, followed by the conclusion.

2. CFD simulation

IEA Wind Task 31 has released three different cases for three different atmospheric stability regimes. In this study, neutral and unstable cases are chosen. The proposed highly-stable case is not considered in this study due to the numerical complexities in the turbulence modeling for the stable atmospheric boundary layer. To reproduce the scenarios, NREL's Simulator fOr Wind Farm Applications (SOWFA) tool [12] is used. SOWFA is a large-eddy simulation (LES) tool that can generate an ABL profile with atmospheric stability, and both an actuator disk model (ADM) and an actuator line model (ALM) are incorporated in the tool to mimic the wind turbine blades. To generate the precursor flows, the simulations are run with a target mean wind speed of 8.7 m/s and 6.7 m/s at hub height 32.1 m for the neutral and unstable cases, respectively. The domain size is 3 km $\times$ 3 km $\times$ 1 km $(x \times y \times z)$ for the neutral case and 4 km $\times$ 3 km $\times$ 2 km $(x \times y \times z)$ for the unstable case, representing the x-mean wind direction, y-transversal direction, and z-vertical direction. Domain sizes are chosen in a way to accommodate the near-surface transient streaks [12]. Details of the mesh for both cases are provided in Table 1. The mesh in the vertical direction of the neutral case is generated with a scaling factor of 2.95 to provide a smaller mesh size that is closer to the surface. A scaling factor of 2.95 provides the target 5 m grid near the surface with a target number of grid points along the vertical direction. The precursor simulation is initiated with a temperature fluctuation of 0.1 K and run with a periodic boundary condition wherein aerodynamic surface roughness, z_0, is 0.01 m. The simulation is tracked with friction velocity, u_*, at the first cell center to see the time requirements for the development of turbulence. The simulation is run up to 16,000 s with a time step of 0.25 s for the neutral case and 12,000 s with a time step of 0.3 s for the unstable case, where the time steps are chosen based on the grid sizes of the cases. Boundary data are saved afterward for 3600 s, and these boundary data are forced to the wind power plant simulation with the pressure gradient calculated from the precursor simulation to have a target mean wind speed at hub height. The precursor data obtained from the simulation are compared with the IEA Wind Task 31 benchmark data in Table 2 and are discussed in detail in Section 4. The domain for the turbine is further refined (Table 2) to capture the wake of the turbine with a substantial resolution. The refined domain covers 16 rotor diameters total along the mean wind direction, which accommodates 6 rotor diameters upstream of the turbine and 10 rotor diameters downstream of the turbine. The turbine model V27 of diameter, $D = 27$ m is mimicked using the ALM in the numerical simulation.

Table 1. Mesh for the simulations

Cases	Precusor mesh size	Turbine domain mesh
Neutral	$\Delta x = 10.0\ m$, $\Delta y = 10.0\ m$, $\Delta z = 5.0\ m$ to $14.8\ m$	$\Delta x = \Delta y = \Delta z = 0.5\ m$
Unstable	$\Delta x = 10.0\ m$, $\Delta y = 10.0\ m$, $\Delta z = 10.0\ m$	$\Delta x = \Delta y = \Delta z = 0.625\ m$

3. Virtual lidar

The SpinnerLidar is a continuous-wave lidar that scans in a rosette pattern and takes approximately 2 s to complete a scan. Each scan provides 984 points in a plane normal to the rotor axis [13]. The lidar is mounted on the nacelle of the turbine and scans downstream of

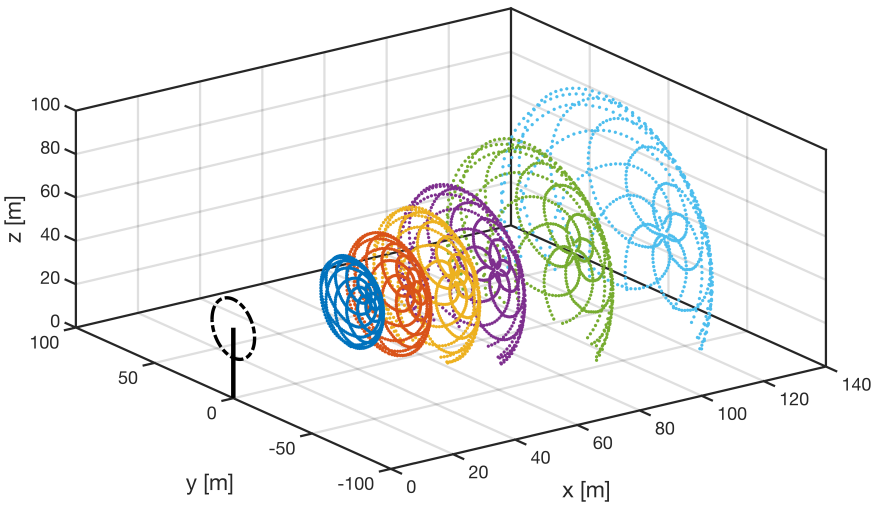

Figure 1. Scan pattern of the virtual lidar placed on the nacelle of the V27 turbine. The lidar is at $x = 0,\ y = 0, and\ z = 32.6$ m.

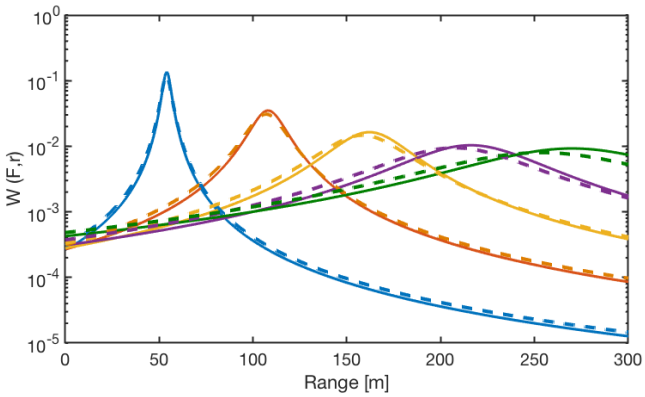

Figure 2. Weighting functions for the continuous-wave lidar. Solid lines represent the Lorentzian weighting function and dashed lines represent the truncated filter function as described by Eq. 6.

the turbine with an angle of 30 degrees maximum to the rotor axis. Rosette measurements in different downstream locations of the turbine are shown in Figure 1. The virtual lidar measures at points in a rosette pattern and provides LOS data according to:

$$v_{\text{los}}(r) = u\cos\phi\cos\theta + v\cos\phi sin\theta + w\sin\phi \tag{1}$$

$$v_{\text{los}}(r) = U_h\cos\phi\cos(\theta - \theta_o) + w\sin\phi \tag{2}$$

where U_h is the horizontal wind speed, r represents the range along the laser beam, ϕ is the elevation angle, θ is the azimuth angle, and θ_o is the wind direction; u, v, and w are the axial, transversal, and vertical velocity components obtained from the numerical simulation, and v_{los} is the LOS data obtained at the corresponding points. Here, the turbine is considered to be

aligned with the wind direction. Total 984×5 points are created in a two-dimensional plane so that each point is surrounded by 4 extra points to reproduce the scenarios of aerosol suspended in the environment and the curvature of the rosette plane (Figure 1). The focus of the converging lidar beams vary to measure at different distances from the lidar, and measurement volume increases with an increase of the measurement distance from the lidar. To consider the volume measurements rather than a point measurement, the weighting function is used for the point measurements. The weighting function is developed considering the laser beam is very narrow in the transversal direction.

$$v_{\text{los,eq}}(F) = \int_0^{\text{inf}} v_{\text{los}}(r) W(F, r) dr \tag{3}$$

where F is the distance along the beam from the lidar to the intended measured point, and $W(F, r)$ is the weighting function. The weighting function for the continuous-wave lidar is described in [14].

The weighting function for the different measured distances is shown in Figure 2. According to [15], axial weighting functions for a continuous-wave monostatic coherent lidar is described by a Lorentzian function:

$$W(F, r) = \frac{1}{\pi} \frac{Z_R}{Z_R^2 + (r - F)^2} \tag{4}$$

where Z_R is the half-width of the weighting function to the $-3\ dB$ point (i.e., 50% of peak sensitivity).

$$Z_R = \frac{\lambda F^2}{\pi \alpha_o^2} \tag{5}$$

where $\lambda = 1565 * 10^{-6}$ mm and $\alpha_o = 24.7$ mm are the laser wavelength and effective telescope radius, respectively.

In addition to the weighting function based on the Lorentzian function, a more physical weighting function is described with a treatment of truncated Gaussian beam with a Lommel function in the complex domain [16]. With a truncation coefficient, light distribution near focus is provided as:

$$W = I_o \left(1 - \frac{0.5 u_a}{\pi N_a}\right)^2 \frac{\alpha^2}{\alpha^2 + (0.5 u_a)^2} \frac{\cosh \alpha - \cos(0.5 u_a)}{\cosh \alpha - 1} \tag{6}$$

$$I_o = \left(\frac{\pi a^2 A}{\lambda F^2} \frac{1 - \exp(-\alpha)}{\alpha}\right)^2 \tag{7}$$

where $A = 1$ is a constant, $a = 44.5$ mm is the aperture radius for the SpinnerLidar, $\alpha = (\frac{a}{w})^2$ is the coefficient of truncation, N_a is a Fresnel number associated with the radius of aperture, w is beam radius at lens, $N_a = \frac{a^2}{F\lambda}$, and $u_a = \frac{2\pi}{\lambda}(\frac{a}{F})^2 \frac{E}{1+E/F}$, $E = r^{-F}$. See [16] for more explanation on these parameters. The purpose of showing these two weighting functions is to emphasize the difference between them. The truncated weighting function is more physical, whereas the Lorentzian weighting function is much simpler. However, the Lorentzian function is effective considering the probe volume of the continuous-wave lidar at different focal distances. As data points are discrete in the considered cases, weighted data are obtained with:

$$v_{\text{los,eq}}(F) = \frac{\sum_{i=1}^{n_p} v_{\text{los}}(r) W(F, r)}{\sum_{i=1}^{np} W(F, r)} \tag{8}$$

where n_p is the number of data points.

4. Results

4.1. ABL data

Atmospheric boundary layer data obtained from the numerical simulations are presented with the horizontal wind speed, U_h, and turbulence intensity with a comparison to the IEA Wind Task 31 SWiFT benchmark data in Table 2. For both cases, numerical simulations underpredict the turbulence intensity compared to the IEA Wind Task 31 validation data, wherein mean U_h agrees well (Figure 3 & 4). A virtual lidar is also added on the top of the nacelle to measure the precursor data at 2.5 rotors upstream distance of the turbine to see the error related to the volume averaging, ϵ_{vol}, and assumptions on the retrieval, ϵ_{pos}, for the both cases. The error due to the volume averaging is defined as:

$$\epsilon_{\text{vol}} = \frac{v_{\text{los}} - v_{\text{los,eq}}}{v_{\text{los}}} * 100 \tag{9}$$

The error due to the retrieval assumption ($w \sin\phi = 0$) is defined as:

$$\epsilon_{\text{pos}} = \frac{U_{h,s} - U_{h,los}}{U_{h,s}} * 100 \tag{10}$$

The total error of the horizontal wind speed retrieved from the virtual lidar is given as:

$$\epsilon_{\text{tot}} = \frac{U_{h,s} - U_{h,eq}}{U_{h,s}} * 100 \tag{11}$$

where $U_{h,s}$ is the horizontal wind speed from the numerical simulation directly, and $U_{h,eq}$ and $U_{h,los}$ are the horizontal wind speed retrieved from $v_{\text{los,eq}}$ and v_{los}, respectively, using Eq. 2 and $w \sin\phi = 0$.

Table 2. Precursor data at hub height

Cases	Parameters	IEA Wind Task 31	Numerical simulations	Virtual lidar
Neutral	U_h (m/s)	8.70	8.84	8.85
	Turbulence Intensity, TI (%)	10.70	9.01	7.55
Unstable	U_h (m/s)	6.70	6.81	6.70
	Turbulence Intensity, TI (%)	12.60	10.95	9.52

Volume averaging results in an error of 16.2% and 13.1% in turbulence intensity at hub height for the neutral and unstable cases, respectively (Table 2), whereas profiles of the horizontal wind speed, U_h, are well-captured within the considered range of heights. However, there is some deviation closer to the surface. This might occur due to the presence of zero LOS data near the surface and propagation of zero value due to the interpolation scheme. In addition, higher vertical velocity closer to the surface plays a role on it. While the error due to the volume averaging is negligible, the percentage of mean absolute error due to the retrieval assumptions, i.e., $w \sin\phi = 0$, is comparatively larger due to the scan with higher elevation angles (Figure 3c).

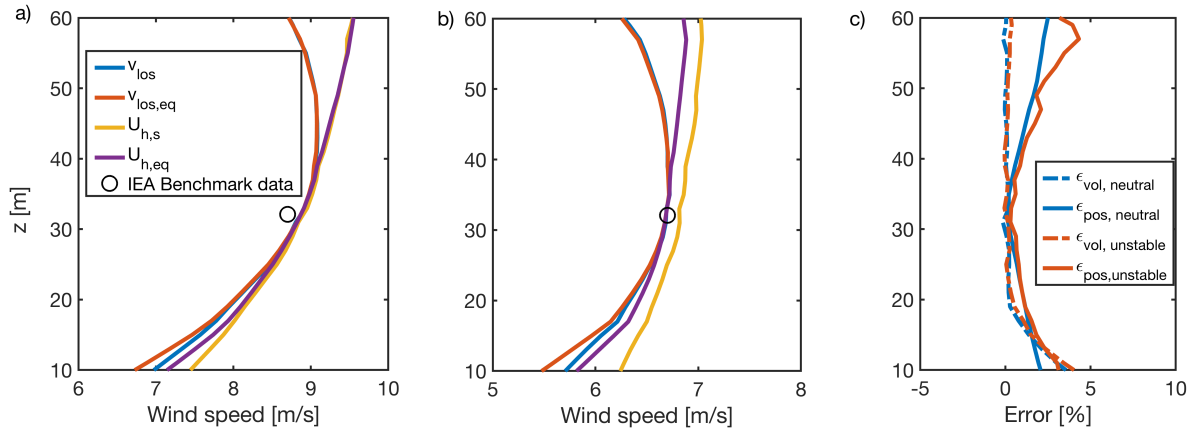

Figure 3. ABL data by virtual lidar with the IEA Wind Task 31 benchmark data. a) neutral case; b) unstable case; c) error due to the volume averaging and retrieval assumption.

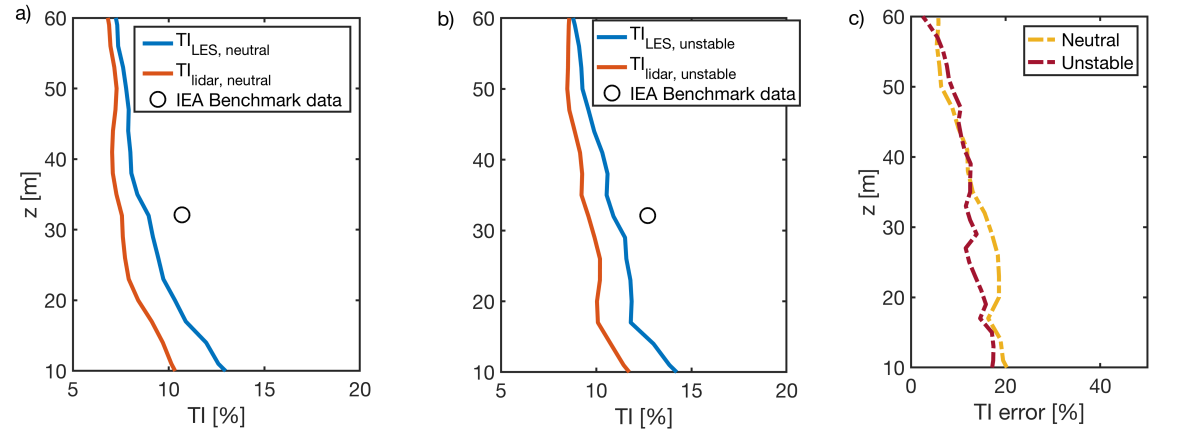

Figure 4. Turbulence intensity data by virtual lidar with the IEA Wind Task 31 benchmark data. a) neutral case; b) unstable case; c) error due to the volume averaging and retrieval assumption.

4.2. Wind turbine wake data

Wind turbine simulations are run for 800 s. The first 200 s of simulated time reflects startup transients of the simulation and not taken into account during the analysis. To capture the wake of the wind turbine with a lidar, a virtual lidar is set to measure 10 rotor diameters downstream ($x = 10D$). While all the data are used to calculate the volume-averaged data at different focal distances, data analysis is done up to $6D$ downstream. The variation of wind speed at different downstream distances is higher in wind turbine wakes compared to the ABL. Therefore, volume averaging might have a significant effect on the wind turbine wake data, and a less significant effect in the ABL. A qualitative view of the volume-averaged data compared to the original LOS data at 3D downstream is shown in Figure 4. In Figure 4c, the difference between LOS data and volume-averaged data explains that volume averaging plays a significant role in the hub and shear layer regions where coherent structures most likely exist. Mean wind speed profiles at $x = 3D$ and $y = 0.0D$ are presented in Figure 7 to show the profiles associated with different errors.

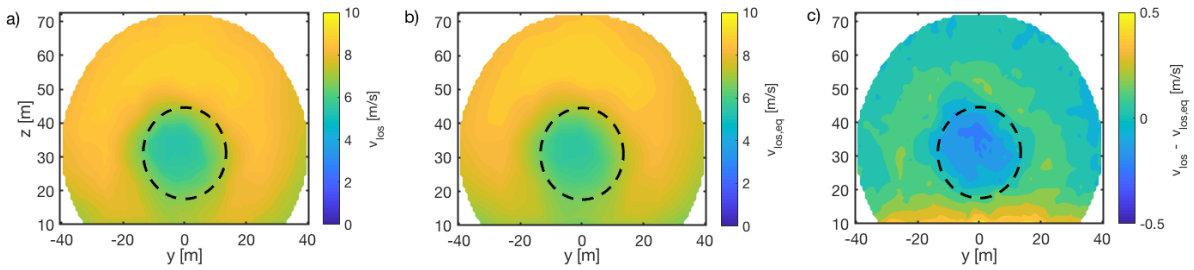

Figure 5. LOS data of the neutral case at 3 rotor diameters downstream (x=3D) from the turbine; a) LOS data; b) weighted LOS data after volume averaging; c) difference between LOS and volume-averaged data. Circle with dashed line represents the rotor area.

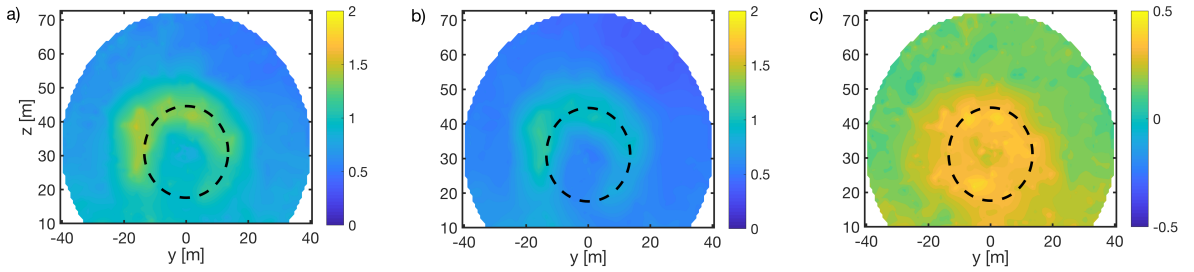

Figure 6. Standard deviation (std. dev.) of the horizontal wind speed in the wake of the neutral case at $x = 3D$; a) std. dev. of $U_{h,s}$; b) std. dev. of $U_{h,eq}$; c) difference between a) and b). Circle with dashed line represents the rotor area.

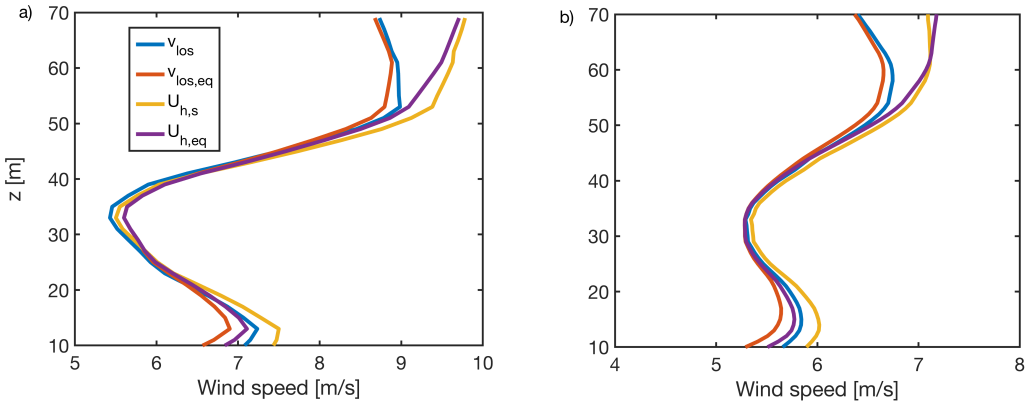

Figure 7. Mean wind speed profile by the virtual lidar compared to the original simulation data at x=3D, y=0.0D; a) neutral case, and b) unstable case.

Effects of volume averaging are quantified for the simulated wakes as in Eq. 9. Figure 5 shows LOS velocity from the simulations compared to the virtual lidar, and their difference. Their difference (Figure 5c) reveals that the virtual lidar measurements are missing the structures located at the hub and tip of the blades region. An error related to the volume averaging is dominant and has a magnitude of 1.95% in the hub region. While the effect of volume averaging does not have a significant impact on the mean velocity profile at $x = 3D$, the impact of volume averaging is significant on the fluctuation of wind speed. The standard deviation of horizontal

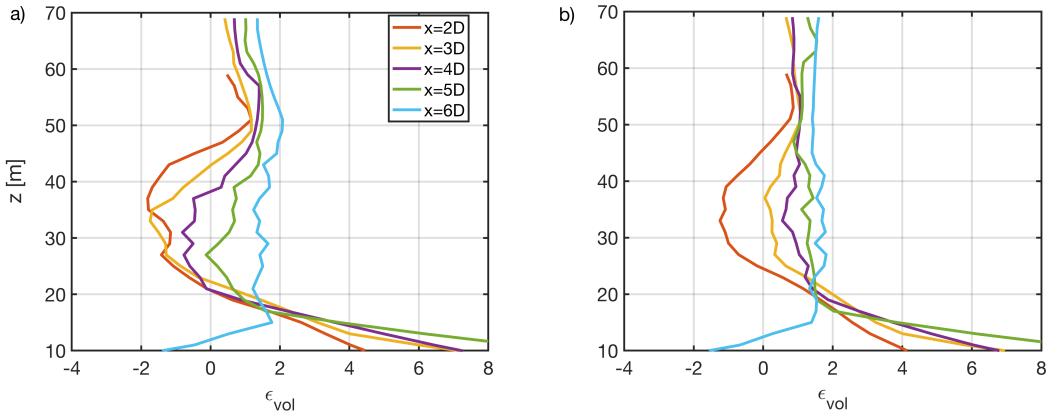

Figure 8. Error introduced by the volume averaging at different downstream locations; a) neutral case, and b) unstable case.

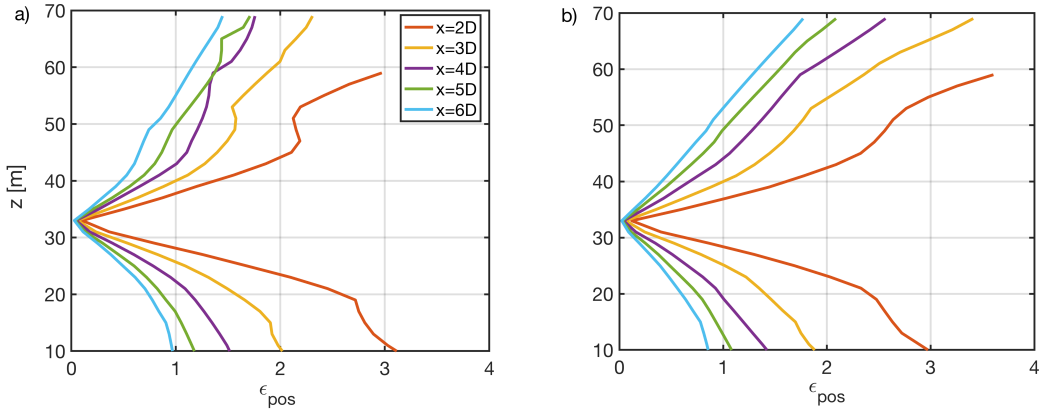

Figure 9. Error introduced by the assumption ($w \sin\phi = 0$) in the retrieval process at different downstream locations; a) neutral case, and b) unstable case.

wind speed is shown in Figure 6. The figure shows that the impact of volume averaging is considerable. More quantitative analysis reveals that volume averaging reduces the standard deviation of 31% at $x = 3D$ and 51% at $x = 5D$ for the neutral case.

In addition, the ϵ_{vol} is presented in Figure 8 for the mean horizontal wind speed at different downstream distances. It is anticipated that an error due to the volume averaging over different downstream distances will increase due to the larger volumes. While the error is concentrated in the shear layer for the near wake, it covers the entire wake area in the far wake ($x = 5D$) due to the mixing of the wake at far distances. The shear layer and coherent structures are dependent on the mixing of the wake, and volume averaging has an impact on it. In addition, wake recovery rate has a significant role in volume averaging due to the variation of wind speed along the weighting function. This can been seen with a comparison between the neutral and unstable cases in Figure 8a and Figure 8b. Volume averaging can underestimate or overestimate the wind speed based on the wake recovery rate and measurement locations of the wake. For the tip regions of the blades, volume averaging always underestimates the wind speed. However, for the hub or center region of the wake, it overestimates in the near wake and underestimates in the far wake region. Sampling volume in the far wake covers a significant portion of the near

wake and underestimates the wind speed for the far wake. While underestimation of the mean wind speed starts at $x = 5D$ for the neutral case, it starts at $x = 3D$ for the unstable case.

Projection error is significant in the near wake for both cases (Figure 9a & Figure 9b), and it decreases with downstream distances. For the same height, the elevation angle decreases with downstream distances and the projection error becomes negligible after $x = 5D$ downstream. The projection error is always higher for the unstable case than the neutral case due to a possible higher vertical velocity in the unstable case. Note that, if the shear layer is thin and coherent, the spike in the projection error is observed at the shear layer (Figure 9a, at $x = 2D$ and $x = 3D$).

5. Conclusion

Large eddy simulations with a virtual lidar are used to study the capabilities of the continuous-wave lidar to measure horizontal wind speed, U_h, and turbulence intensity, TI, in both the atmospheric boundary layer (ABL) and wind turbine wake. Two different cases (neutral and unstable) are chosen based on the IEA Wind Task 31 SWiFT Benchmark and virtual lidars are placed on the nacelle of the turbine at a hub height of 32.1 m. The virtual lidar captures the mean, U_h, well from height 10 m to 70 m in the ABL. However, it underestimates the turbulence intensity for both the ABL and wind turbine wake. The underestimation of turbulence intensity is significant in the wake, and it could be more than 50% at $x = 5D$. This reduction is directly related to the sampling volume considered by the lidar. The mean U_h is well-captured up to $x = 3D$ in the wake with a projection error less than 2.5%. However, after $x = 5D$, the error related to the volume averaging becomes prominent and significant deviations in the mean, U_h, were observed. At $x = 5D$, the error associated with volume averaging is significant for the unstable case due to the faster wake recovery. The faster wake recovery and mixing in the wake create a larger variation of wind speed in the sample volume. The lidar overestimates the wind speed in the near wake and underestimates the wind speed in the far wake. The location of the transition from an overestimation to an underestimation of wind speed in the wake is dependent on the wake recovery rate. For both cases, projection error in the wake decreases with downstream distances and an error due to the volume averaging increases with downstream distances. Volume averaging is dominant in the shear layer of the wake for the mean, U_h, and all over the wake for the turbulence intensity.

6. Acknowledgments

This work was authored [in part] by the National Renewable Energy Laboratory, operated by Alliance for Sustainable Energy, LLC, for the U.S. Department of Energy (DOE) under Contract No. DE-AC36-08GO28308. Funding provided by the U.S. Department of Energy Office of Energy Efficiency and Renewable Energy Wind Energy Technologies Office. The views expressed in the article do not necessarily represent the views of the DOE or the U.S. Government. The U.S. Government retains and the publisher, by accepting the article for publication, acknowledges that the U.S. Government retains a nonexclusive, paid-up, irrevocable, worldwide license to publish or reproduce the published form of this work, or allow others to do so, for U.S. Government purposes. Sandia National Laboratories is a multimission laboratory managed and operated by National Technology & Engineering Solutions of Sandia, LLC, a wholly owned subsidiary of Honeywell International Inc., for the U.S. Department of Energy's National Nuclear Security Administration under contract DE-NA0003525. Matthew Churchfield is acknowledged for implementing the virtual lidar function in the Simulator fOr Wind Farm Applications (SOWFA) code.

References

[1] Nikola Vasiljevic, Michael Courtney, and Jakob Mann. PhD thesis, Denmark, 2014.

[2] J. K. Lundquist, M. J. Churchfield, S. Lee, and A. Clifton. *Atmospheric Measurement Techniques (Online)*, 8(2), 2 2015.
[3] Mikael Sjöholm, Torben Mikkelsen, Jakob Mann, Karen Enevoldsen, and Michael Courtney. *Meteorologische Zeitschrift*, 18(3):281–287, 06 2009.
[4] A. Sathe, J. Mann, J. Gottschall, and M. S. Courtney. *Journal of Atmospheric and Oceanic Technology*, 28(7):853–868, 2011.
[5] Alfredo Pena Diaz, Mikael Sjöholm, Torben Krogh Mikkelsen, and Charlotte Bay Hasager. *Journal of Physics: Conference Series*, 2018.
[6] A. R. Meyer Forsting, N. Troldborg, and A. Borraccino. *Journal of Physics: Conference Series*, 854(1), 2017.
[7] C L Kelley, T G Herges, L A Martinez, and T Mikkelsen. *Journal of Physics: Conference Series*, 1037:052014, jun 2018.
[8] Paula Doubrawa, Rebecca J. Barthelmie, Hui Wang, and Matthew J. Churchfield. *Wind Energy*, 20(3):449–463, 2017.
[9] Paula Doubrawa, Rebecca J. Barthelmie, Hui Wang, S. C. Pryor, and Matthew J. Churchfield. *Remote Sensing*, 8(11), 2016.
[10] T. Mikkelsen, N. Angelou, K. Hansen, M. Sjöholm, M. Harris, C. Slinger, P. Hadley, R. Scullion, G. Ellis, and G. Vives. *Wind Energy*, 16(4):625–643, 2013.
[11] P Doubrawa, M Debnath, P J Moriarty, E Branlard, T G T Herges, C Kelley, D C Maniaci, and Naughton B. *Journal of Physics: Conference Series*, 2019.
[12] Matthew J. Churchfield, Sang Lee, John Michalakes, and Patrick J. Moriarty. *Journal of Turbulence*, 13:N14, 2012.
[13] M Churchfield, Q Wang, A Scholbrock, T Herges, T Mikkelsen, and M Sjöholm. *Journal of Physics: Conference Series*, 753:032009, sep 2016.
[14] E Simley and L Y Pao. Technical report, NREL, 2012.
[15] Chris Slinger and Michael Harris. *Proc. Summer School in Remote Sensing for Wind Energy*, pages 1–32, 2012.
[16] Zoltán L Horváth and Zsolt Bor. *Optics Communications*, 222(1):51 – 68, 2003.